Near-lossless method for generating thermal photon-bunched light

Xi Jie Yeo,[1] Darren Ming Zhi Koh,[1] Justin Yu Xiang Peh,[1] Christian Kurtsiefer,[1,2] and Peng Kian Tan[1, a)]
[1)] *Centre for Quantum Technologies, 3 Science Drive 2, Singapore 117543*
[2)] *Department of Physics, National University of Singapore, 2 Science Drive 3, Singapore, 117551*

(Dated: 24 November 2026)

Thermal light sources exhibiting photon bunching have been suggested for sensing applications that exploit timing correlations of stationary light, including range finding, clock synchronization, and non-line-of-sight imaging. However, these proposals have remained unrealized in practice because available sources of photon bunching either possess coherence times too short to be timing resolved by photodetectors, or produce brightness levels too low to tolerate realistic return losses. In this work, we demonstrate a low-loss method for generating photon bunching with a conversion efficiency nearly 9 orders of magnitude higher than that achieved by many other bunching processes.

I. INTRODUCTION

Many sensing methods with non-classical light generated by parametric conversion mostly rely on the tight temporal correlation of photon pairs[1]. However, significant temporal correlation between photodetection times can also be found in thermal light[2]. Blackbody radiation provides a natural source of thermal photon bunching, with Sunlight filtered at 546 nm exhibiting a spectral density comparable to that of a low-pressure Mercury vapor discharge lamp, on the order of 10^7 photoevents per second per nanometer per mode. For sensing applications, such as LIDAR, much brighter sources are necessary to overcome high return losses in these scenarios[10].

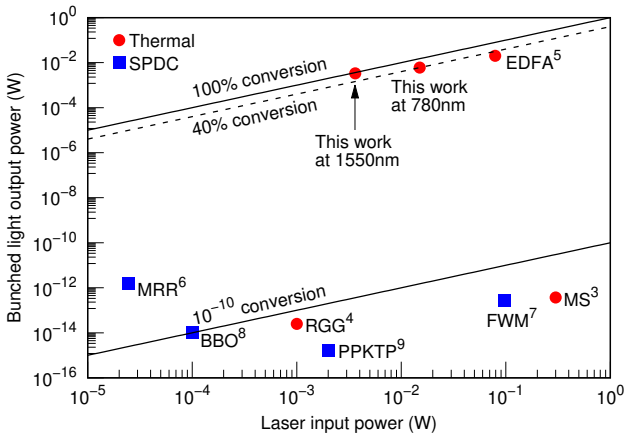

FIG. 1. Power relations of various methods and for generating photon-bunched light from laser light: MS[3] – liquid suspension of microspheres, RGG[4] – rotating ground glass, EDFA[5] – Erbium-doped fiber amplifier. Methods based on parametric conversion: MRR[6] – cavity enhanced via microring resonator, FWM[7] – four-wave mixing, BBO[8] – downconversion in β-Barium Borate crystal, PPKTP[9] – downconversion in periodically polled Potassium Titanyl Phosphate crystal

[a)] Electronic mail: pengkian@gmail.com

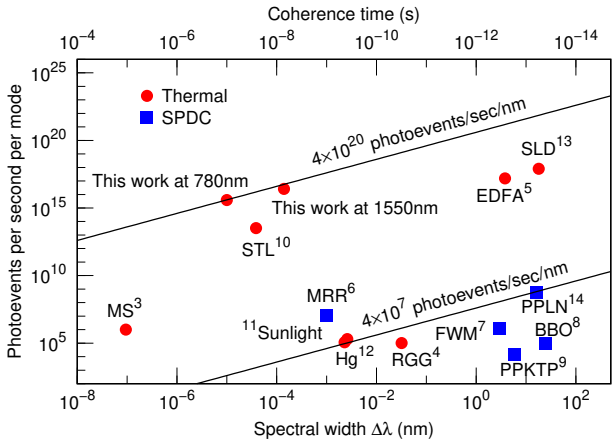

FIG. 2. Spectral densities of stationary light sources exhibiting photon-bunching correlations. Apart from the demonstrations referenced in Fig. 1, other demonstrations shown are: STL[11] – subthreshold laser diode,[12] – filtered Sunlight, Hg[13] – Mercury discharge lamp, SLD[14] – superluminescent diode, PPLN[15] – parametric down conversion in periodically poled Lithium Niobate.

These can be based on conversion of coherent laser light into photon-bunched light[3–9] (see Fig. 1). Already established methods, commonly referred to as sources of 'pseudothermal light', rely on scattering coherent laser light from random phase-dispersive media, such as a rotating ground glass, or a liquid suspension of microspheres in Brownian motion.

The scattering processes in these methods introduce speckle patterns that are spatially multimode. These scattering-induced fluctuations lead to highly inefficient coupling to single spatial optical modes, reducing the intensity of bunched light by approximately 10 orders of magnitude relative to the input laser. Photon bunched light can also be prepared through spontaneous parametric down-conversion (SPDC) processes, which are similarly inefficient.

Erbium-doped fiber amplifiers (EDFA) operating below their lasing threshold can reach relatively high conversion efficiency, transforming about 25% of the 980 nm

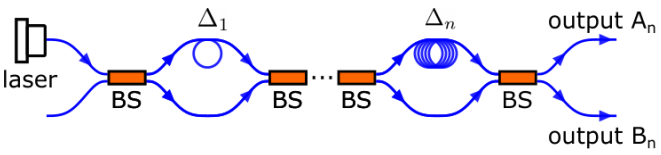

FIG. 3. A scheme to efficiently generate thermal photon-bunched light from coherent laser light by using a cascaded series of asymmetric Mach-Zehnder fiber interferometers. The input field is first split by a beamsplitter (BS), with one arm acquiring a propagation delay Δ_1 before recombination at a subsequent beamsplitter with the non-delayed arm. The interferometric loop can be repeated n times, with each stage introducing progressively longer fiber delays Δ_n, providing two single-mode outputs (A_n, B_n).

pump laser into amplified spontaneous emission centered around 1550 nm. However, the resulting output thermal light is spectrally broad, spanning several tens of nanometers, with a correspondingly short sub-picosecond coherence time that cannot be readily resolved by conventional photodetectors for observing photon bunching. Moreover, the accessible conversion wavelengths are inherently restricted by the available amplification media. A chart of the relationship between spectral bandwidth and photon output per optical mode for demonstrated photon-bunched light sources is shown in Fig. 2.

Here, we demonstrate a wavelength-independent technique for generating spectrally narrowband photon-bunched light from laser light. In principle, the process can approach near-unity conversion efficiency, as it is free from the fundamental losses typically associated with mode mismatch in scattering processes.

II. IDEA

Thermal light can be modeled as an ensemble of phase-independent coherent fields[2]. To generate thermal photon-bunched light from laser light, a scheme is required to transform the laser emission into a micro-ensemble of mutually phase-independent fields. We rely on the random phase relation of typical laser light at time differences outside the coherence time of the laser. The conversion can be realized by cascading a series of asymmetric Mach-Zehnder interferometers, each introducing an additional propagation delay Δ_n in one arm (see Fig. 3). The accumulated delays randomize the relative phases of the component fields without introducing scattering losses. This scheme can be implemented in single-mode optical fibers, suppressing the losses from mode mismatch compared to a free-space implementation.

The electric field amplitude of the input laser light can be described by

$$E(t) = E_0 e^{i[2\pi f t + \phi(t)]}\,, \tag{1}$$

where E_0 denotes the constant electric field amplitude, f the laser frequency, and $\phi(t)$ the time-dependent phase fluctuation capturing the finite coherence time of the laser[16].

After the light passes through the first interferometer with an additional delay of Δ_1 in one arm, the electric field amplitudes (for matching polarizations at the second beamsplitter) at outputs A_1, B_1 are

$$E_{A_1,B_1}(t) = \frac{1}{2}[E(t) \pm E(t-\Delta_1)]\,, \tag{2}$$

with the difference between the two outputs caused by the relative π phase shift imparted by any beamsplitter.

Passing both output fields through the next interferometer with a corresponding delay Δ_2 produces the following field amplitudes (for matching polarizations) at outputs A_2, B_2:

$$\begin{aligned} E_{A_2,B_2}(t) =& \frac{1}{2\sqrt{2}}[E(t) - E(t-\Delta_1) \mp E(t-\Delta_2) \\ & \mp E(t-\Delta_1-\Delta_2)]\,. \end{aligned} \tag{3}$$

These light fields are a superposition of the initial laser field $E(t)$ with delayed copies of itself through a combination of delays Δ_1, Δ_2.

Repeating this procedure through n cascaded interferometers leads to output fields that are superpositions of the original coherent field and all delayed copies generated by the full set of delays $\{\Delta_1, \Delta_2, ..., \Delta_n\}$,

$$\begin{aligned} E_{A_n}(t) =& \frac{1}{\sqrt{2}^{n+1}}\Big[E(t) + \sum_{j=1}^{n} \alpha_j E(t-\Delta_j) \\ & + \sum_{j=1}^{n-1}\sum_{k=j+1}^{n} \alpha_{jk} E(t-\Delta_j-\Delta_k) \\ & + \sum_{j=1}^{n-2}\sum_{k=j+1}^{n-1}\sum_{l=k+1}^{n} \alpha_{jkl} E(t-\Delta_j-\Delta_k-\Delta_l) \\ & + \cdots \\ & + E(t-\Delta_1-\cdots-\Delta_n)\Big]\,, \end{aligned} \tag{4}$$

with all coefficients $\alpha \in \{1, -1\}$. A similar expansion holds for E_{B_n}. The resulting output fields are superpositions of the initial laser light field $E(t)$ together with the $2^n - 1$ delayed copies of itself that passed through different combinations of delays Δ_1 to Δ_n.

To ensure phase independence between the various delayed copies of the initial light field $E(t)$, the delays Δ_n in each interferometric loop n are chosen to satisfy

$$\Delta_n - \Delta_{n-1} \geq \tau_c, \tag{5}$$

such that each successive delay exceeds the laser coherence time τ_c.

According to the Wiener-Khinchin Theorem, the autocorrelation function of a stationary signal is given by the Fourier transform of its power spectral density. A laser

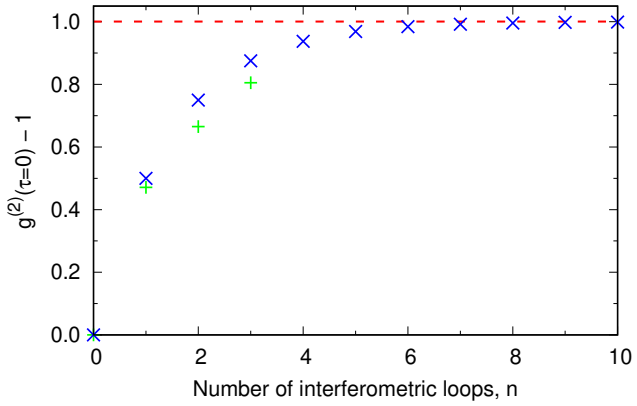

FIG. 4. Photon bunching peak amplitude $g^{(2)}(\tau=0)-1 = 1-\frac{1}{2^n}$, scaling with the number of interferometric loops n, as described by a simplified form of Eq. (6) where $\tau = 0$. The blue $\times$ symbols denote the theoretical bunching peak amplitudes corresponding to integer values of n. Green $+$ symbols mark bunching peak amplitudes obtained experimentally up to $n = 3$. The horizontal red dashed line indicates the photon bunching amplitude $g^{(2)}(0)-1 = 1$ expected for ideal thermal light.

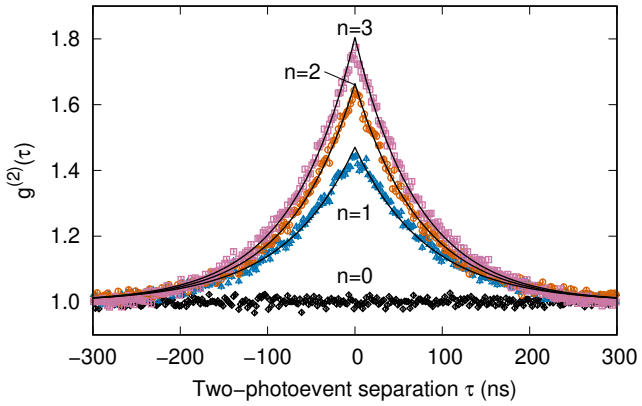

FIG. 5. Photon bunching signatures from a laser light (center wavelength $\lambda = 780\,\text{nm}$) passing through a number n of asymmetric Mach-Zehnder interferometers. A numerical fit to a double-exponential decay reaches a peak value of the second order correlation function at time delay $\tau = 0$. We find for $n = 0$ (no interferometer): $g^{(2)}(\tau) = 1$, for $n = 1$: $g^{(2)}(0) = 1.471 \pm 0.003$, for $n = 2$: $g^{(2)}(0) = 1.665 \pm 0.003$, and for $n = 3$: $g^{(2)}(0) = 1.805 \pm 0.004$. The coherence times extracted for all traces is around $\tau_c \approx 135\,\text{ns}$ (see text for details).

with a Lorentzian spectral line shape[2] therefore exhibits a first-order coherence function $g^{(1)}(\tau)$ proportional to $e^{-\tau/\tau_c}$, whereby $1/\tau_c$ is the corresponding laser linewidth.

The output is therefore an ensemble of 2^n phase-independent coherent fields. As a result, the light exhibits thermal photon bunching characterized by the second-order coherence function:

$$g^{(2)}(\tau) - 1 = \left(1 - \frac{1}{2^n}\right) e^{-2|\tau|/\tau_c}. \qquad (6)$$

The photon bunching amplitude increases with the number of interferometric loops n, converging to $g^{(2)}(0)-1 = 1$ for an infinite number of phase-independent light fields, matching the correlation of an ideal thermal light source (see Fig. 4).

Realistic systems may not meet the power balance assumption in Eq. (2) for various reasons. This will reduce the photon bunching amplitude (See Appendix).

III. EXPERIMENTAL IMPLEMENTATION

To demonstrate the idea, we inject light from a distributed feedback laser providing linearly polarized light with a center wavelength of 780 nm into a single spatial mode optical fiber and couple this to a fiber beamsplitter separating it into two modes. The first asymmetric Mach-Zehnder interferometer passes light through an additional optical fiber to introduce a propagation delay Δ_1 in one arm with an additional optical fiber of $l_1 = 100\,\text{m}$ length (corresponding to $\Delta_1 \approx 495\,\text{ns}$), exceeding the laser coherence time τ_c, and another fiber beam splitter closing the interferometer.

A passive paddle polarization controller (not shown in Fig. 3) ensures the simple form of adding amplitudes in Eq. (2). Polarization in the interferometer legs are relatively stable after initial setup and thus no active polarization control was used. Additionally, variable attenuators are inserted in the short leg of the interferometer to compensate for losses in the delay fibers, thereby balancing light intensities just prior to mode-overlap at the subsequent beamsplitters. These parameters are optimized to increase the interferometric visibility; the maximum of the photon bunching signature $g^{(2)}(\tau = 0)$ is taken as an optimization criterion for polarization and intensity balancing control.

To chain the delay combination, more asymmetric Mach-Zehnder interferometers are added, as well as polarization and intensity balance components. The delay fiber lengths ($l_2 = 186\,\text{m}$, $l_3 = 500\,\text{m}$) are chosen to introduce propagation delays Δ_n in each loop that closely satisfy the condition in Eq. (5).

To perform the $g^{(2)}(\tau)$ timing correlation measurements, light from either output A_n or B_n is collected by a pair of actively quenched Silicon avalanche photodetectors. The resulting photodetection events are timestamped with a time resolution of 2 ns.

IV. RESULTS

To show the photon bunching signature, the temporal correlation functions $g^{(2)}(\tau)$ for different numbers n of interferometers were numerically extracted from the stream of detector time stamps, and are shown in Fig. 5.

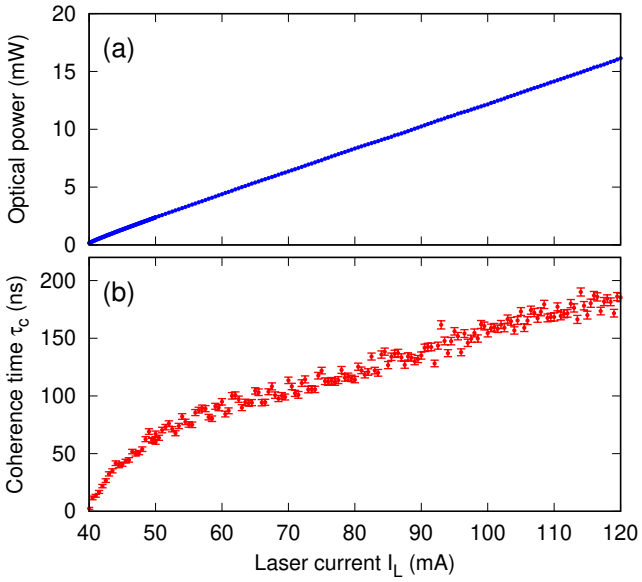

FIG. 6. Tunable (a) output photon bunching power and (b) coherence time τ_c by adjusting the laser injection current I_L.

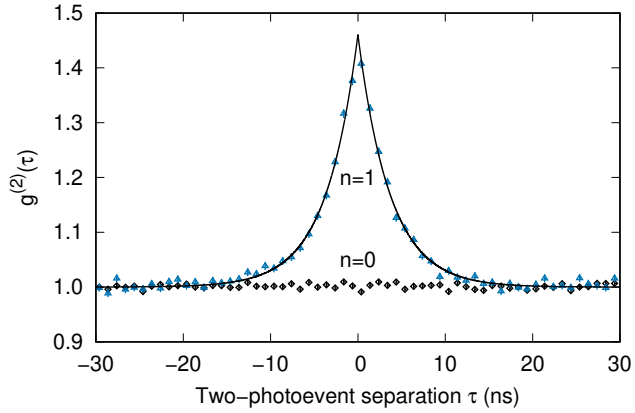

FIG. 7. Photon bunching signature from laser light ($\lambda = 1550\,\text{nm}$) passing through $n = 1$ interferometer. Numerical fitting gives a peak $g^{(2)}(\tau = 0) = 1.461 \pm 0.006$ with a coherence time of $\tau_c = 7.4 \pm 0.2\,\text{ns}$.

As a reference, a flat $g^{(2)}(\tau) = 1$ is observed for $n = 0$ (i.e., no interferometer) which is consistent with the unbunched Poisson statistics expected from a laser emitting coherent light. The resultant photon bunching peaks for $n > 0$ were fitted to two-sided exponential decays (as expected for Lorentzian line shapes of the laser light), using a model function $g^{(2)}(\tau) = 1 + b \cdot e^{-2|\tau|/\tau_c}$. For $n = 1$, we obtain $g^{(2)}(0) = 1.471 \pm 0.003$ with a coherence time of $\tau_c = 135.6 \pm 0.3\,\text{ns}$. For $n = 2$, we obtain $g^{(2)}(0) = 1.665 \pm 0.003$ and $\tau_c = 134.8 \pm 0.2\,\text{ns}$, for $n = 3$, $g^{(2)}(0) = 1.805 \pm 0.004$ and $\tau_c = 135.2 \pm 0.2\,\text{ns}$, respectively. This suggests that the correlation function converges towards $g^{(2)}(\tau = 0) = 2$ with increasing number n of interferometers (providing an increasing number of phase-independent effective light sources with the same spectrum). This behavior closely approximates the statistics of an ideal thermal light source with photon bunching characteristics $g^{(2)}(\tau) = 1 + e^{-2|\tau|/\tau_c}$. A comparison of the experimentally obtained photon bunching amplitude against the theoretical value expected can be seen in Fig. 4.

The coherence time τ_c of the laser used was long, which conveniently allowed us to resolve the exponential decay of the correlation function from the thermal bunching peak. We can also vary the coherence time by adjusting the injection current to the laser diode. In Fig. 6, we show the dependence of the laser power and coherence time τ_c. For injection currents slightly above the lasing threshold (around 40 mA), the laser emits very little power and has a short coherence time. With increasing injection current, the output power of the laser increases, as well as the coherence time extracted from the decay of $g^{(2)}(\tau)$. Therefore, the presented technique also allows control over the temporal coherence time, complementing the control over the photon bunching amplitude $g^{(2)}(\tau = 0)$ with the number n of asymmetric Mach-Zehnder interferometers.

For $n = 1$, we observe a conversion efficiency from laser light to photon-bunched light at both output ports together of 40%. This loss is mostly contributed by the high losses in our delay fiber at 780 nm wavelength, and the corresponding attenuation to balance the intensity in both interferometer arms. A significantly higher conversion efficiency can be obtained when moving to a wavelength where optical fibers have a lower loss.

With a similar experimental setup at the telecommunication wavelength of 1550 nm, we observe a combined power from both output ports of 3.36 mW from an initial input power 3.63 mW, corresponding to a conversion efficiency of 92.5%. A clear photon bunching peak can also be seen with $g^{(2)}(\tau = 0) = 1.461 \pm 0.006$ with a coherence time of $\tau_c = 7.4 \pm 0.2\,\text{ns}$ as shown in Fig. 7.

V. CONCLUSION AND OUTLOOK

We demonstrated a technique to generate thermal photon bunching that is about 9 orders of magnitude more efficient than many other thermal or parametric down conversion processes, showing a photon pair timing correlation that could have applications that rely on time correlations between two photons with an intrinsic randomness of single-photon timings. Moreover, this method also allows for control over the peak photon bunching signature and temporal coherence. If optical wavelengths are used that lead to negligible losses in the asymmetric interferometers, an almost unit conversion efficiency of laser light to photon-bunched light can be reached, providing an unprecedented brightness of photon-bunched light. This efficiency and tunability enable the sensing system to tolerate high return losses in realistic envi-

ronments, thereby opening a pathway toward practical sensing implementations such as range finding, clock synchronization, and non-line-of-sight imaging.

ACKNOWLEDGMENTS

This research is supported by the Quantum Engineering Programme through NRF2021-QEP2-03-P02, the Ministry of Education, and the National Research Foundation, Prime Minister's Office, Singapore.

AUTHOR DECLARATIONS

Conflict of Interest

The authors have no conflicts to disclose.

DATA AVAILABILITY

The data that supports the findings of this study are available from the corresponding author upon reasonable request.

Appendix A: Appendix: light power imbalance in the interferometers

In the derivation of the second order correlation function Eq. (6) in Sec. II we assumed a balanced optical power in the two arms of each interferometer (Eq. (2)). Practical power imbalances, e.g., due to different losses in delay fibres, affect the resulting bunching signature. The expression for the resulting second-order correlation function

$$g^{(2)}(\tau) = \frac{\langle E^*(t)E^*(t+\tau)E(t)E(t+\tau)\rangle}{\langle E^*(t)E(t)\rangle} \tag{A1}$$

would need to use a modified electric field compared to Eq. (4). We exemplify this with a simple example. Consider a single interferometric loop ($n = 1$) comprising two beam paths. If we normalize $\langle E^*(t)E(t)\rangle = 1$, and assign relative powers η and $1-\eta$ in the two paths (corresponding to fields $E_A = \sqrt{\eta}$ and $E_B = \sqrt{1-\eta}$, respectively), such that the interesting power ratio η ranges from 0 to 0.5. Then, the second-order correlation function $g^{(2)}(\tau)$ becomes:

$$\begin{aligned} g^{(2)}(\tau) &= \langle E^*(t)E^*(t+\tau)E(t)E(t+\tau)\rangle \\ &= \sum_{j,k,l,m=A}^{B} \left\langle E_j^*(t)E_k^*(t+\tau)E_l(t)E_m(t+\tau)\right\rangle , \end{aligned} \tag{A2}$$

summing over the contributions of the two arms A, B. The remaining non-zero terms comprise:

$$\begin{aligned} &\sum_{A}^{B} \left\langle E_j^*(t)E_j^*(t+\tau)E_j(t)E_j(t+\tau)\right\rangle = \\ &\qquad = \sqrt{\eta}^4 + \sqrt{1-\eta}^4 \\ &\qquad = \eta^2 + (1-\eta)^2 , \end{aligned} \tag{A3}$$

$$\begin{aligned} &\sum_{j,k=A}^{B} \left\langle E_j^*(t)E_k^*(t+\tau)E_j(t)E_k(t+\tau)\right\rangle = \\ &\qquad = \sqrt{\eta}^2\sqrt{1-\eta}^2 + \sqrt{1-\eta}^2\sqrt{\eta}^2 \\ &\qquad = 2\eta(1-\eta) , \end{aligned} \tag{A4}$$

and

$$\begin{aligned} &\sum_{j,k=A}^{B} \left\langle E_j^*(t)E_k^*(t+\tau)E_k(t)E_j(t+\tau)\right\rangle = \\ &\qquad = \left(\sqrt{\eta}^2\sqrt{1-\eta}^2 + \sqrt{1-\eta}^2\sqrt{\eta}^2\right)|g^{(1)}(\tau)|^2 \\ &\qquad = 2\eta(1-\eta)|g^{(1)}(\tau)|^2 . \end{aligned} \tag{A5}$$

Summing up the non-zero contributions results in the description of the photon bunching dependence on the power ratio η in combining two phase-independent light beams:

$$\begin{aligned} g^{(2)}(\tau) &= \eta^2 + (1-\eta)^2 + 2\eta(1-\eta) + 2\eta(1-\eta)|g^{(1)}(\tau)|^2 \\ &= 1 + 2\eta(1-\eta)|g^{(1)}(\tau)|^2 \end{aligned} \tag{A6}$$

A graphical representation for different power ratios η is shown in Fig. 8(a). The dynamics of temporal photon bunching in excess of the random Poissonian floor can be described simply by $2\eta(1-\eta)$.

Additional reductions of the photon bunching signature can be expected from other contributions to interferometer amplitude imbalance, e.g., a limited mode matching or a polarization mismatch. Fig. 8(b) shows measured photon bunching amplitudes, increasing with a better power matching in the two arms. However, the interferometric visibility $|g^{(1)}(\tau)|$ of the source laser and other instrumentation imperfections might account for the deviation of experimental data points from the theoretical curve in Fig. 8(b).

A more general adaptation of different power imbalances in multiple interferometers ($n > 1$) can be treated in a similar way as exemplified here to generalize the electric field expression Eq. (2).

[1] A. S. Clark, M. Chekhova, J. C. F. Matthews, J. G. Rarity, and R. F. Oulton, "Special topic: Quantum sensing with correlated light sources," Applied Physics Letters **118**, 060401 (2021).
[2] R. Loudon, *The Quantum Theory of Light* (Oxford Science Publications, 2000).
[3] D. Dravins, T. Lagadec, and P. D. Nunẽz, "Optical aperture synthesis with electronically connected telescopes," Nat. Commun. **6**, 6852 (2015).

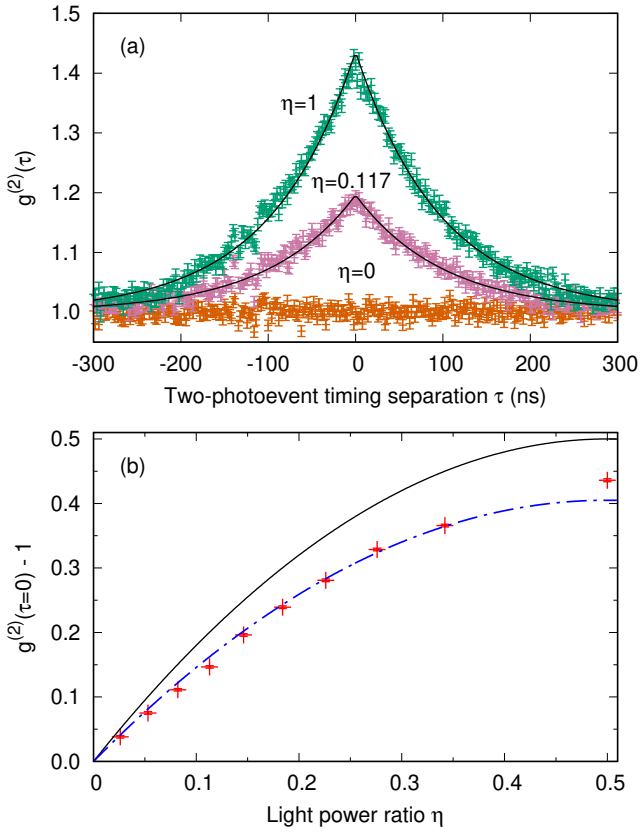

FIG. 8. (a) Second-order timing correlation $g^{(2)}(\tau)$ extracted from the output of a single-loop asymmetric Mach-Zehnder interferometer, with different light power ratios η incident at the second beamsplitter: $\eta = 0.5 : 0.5 = 1$ (green), $\eta = 0.15 : 0.85 = 0.117$ (purple), and $\eta = 0 : 1 = 0$ (orange). (b) The photon bunching amplitude, $g^{(2)}(0) - 1$, scales with different power contributions by the non-delayed light field $E(t)$ over the total output. The red datapoints show the bunching peaks $g^{(2)}(0) - 1$ fitted from the measurements of $g^{(2)}(\tau)$ at varying power ratios. The black solid curve shows the ideal scaling relationship between $g^{(2)}(0)-1$ against the light power ratio η. The blue dashed curve shows the dependency with a visibility of 0.9 adjustment.

[4] J. Zhu, X. Chen, P. Huang, and G. Zeng, "Thermal-light-based ranging using second-order coherence," Appl. Opt. **51**, 4885–4890 (2012).

[5] P. Janassek, A. Herdt, S. Blumenstein, and W. Elsaber, "Ghost spectroscopy with classical correlated amplified spontaneous emission photons emitted by an erbium-doped fiber amplifier," Appl. Sci. **8(10)**, 1896 (2018).

[6] T. J. Steiner, J. E. Castro, L. Chang, Q. Dang, W. Xie, J. Norman, J. E. Bowers, and G. Moody, "Ultrabright entangled photon pair generation from an algaas on insulator microring resonator," Phys. Rev. X Quantum **2**, 010337 (2021).

[7] D. G. England, B. Balaji, and B. J. Sussman, "Quantum-enhanced standoff detection using correlated photon pairs," Phys. Rev. A **99** (2019), https://doi.org/10.1103/PhysRevA.99.023828.

[8] A. Lohrmann, A. Villar, A. Stolk, and A. Ling, "High fidelity yield stop collection for polarization-entangled photon pair sources," Appl. Phys. Lett. **113**, 171109 (2018).

[9] Y.-C. Jeong, K.-H. Hong, and Y.-H. Kim, "Bright source of polarization-entangled photons using a ppktp pumped by a broadband multi-mode diode laser," Opt. Express **24(2)**, 1165–1174 (2016).

[10] U. Wandinger, "Introduction to lidar," in *Lidar: range-resolved optical remote sensing of the atmosphere* (Springer, 2005) pp. 1–18.

[11] P. K. Tan, X. J. Yeo, A. Z. W. Leow, L. Shen, and C. Kurtsiefer, "Practical range sensing with thermal light," Phys. Rev. Appl. **20** (2023), https://doi.org/10.1103/PhysRevApplied.20.014060.

[12] P. K. Tan, A. H. Chan, and C. Kurtsiefer, "Optical intensity interferometry through atmospheric turbulence," MNRAS **457**, 4291–4295 (2016).

[13] P. K. Tan, G. H. Yeo, H. S. Poh, A. H. Chan, and C. Kurtsiefer, "Measuring temporal photon bunching in blackbody radiation," ApJL **789**, L10 (2014).

[14] A. T. M. A. Rahman and P. F. Barker, "Optical levitation using broadband light," Optica **7(8)**, 906–912 (2020).

[15] Z. Zhang, S. Mouradian, F. N. C. Wong, and J. Shapiro, "Entanglement enhanced sensing in a lossy and noisy environment," Phys. Rev. Lett. **114**, 110506 (2015).

[16] L. Mandel, "Fluctuations of photon beams: The distribution of the photo-electrons," Proceedings of the Physical Society **74**, 233 (1959).